[1]*Department of Physics, University of Colorado, Boulder, CO 80309, USA*
[2]*Liquid Crystal Materials Research Center, University of Colorado, Boulder, CO 80309, USA*
[3]*Department of Electrical, Computer, and Energy Engineering and Materials Science and Engineering Program, University of Colorado, Boulder, CO 80309, USA*
[4]*Renewable and Sustainable Energy Institute, National Renewable Energy Laboratory and University of Colorado, Boulder, CO 80309, USA*
[*] *ivan.smalyukh@colorado.edu*

tetyn f tAmercal Oscillatory and excitable systems commonly exhibit formation of dynamic non-equilibrium patterns. For example, rotating spiral patterns are observed in biological, chemical, and physical systems ranging from organization of slime mold cells to Belousov-Zhabotinsky reactions, and to crystal growth from nuclei with screw dislocations. Here we describe spontaneous formation of spiral waves and a large variety of other dynamic patterns in anisotropic soft matter driven by low-intensity light. The unstructured ambient or microscope light illumination of thin liquid crystal films in contact with a self-assembled azobenzene monolayer causes spontaneous formation, rich spatial organization, and dynamics of twisted domains and topological solitons accompanied by the dynamic patterning of azobenzene group orientations within the monolayer. Linearly polarized incident light interacts with the twisted liquid crystalline domains, mimicking their dynamics and yielding patterns in the polarization state of transmitted light, which can be transformed to similar dynamic patterns in its intensity and interference color. This shows that the delicate light-soft-m.3(nzl()-4.5(115 TD[l)-4.3(n-4.3(can)-4.3( )yiel)-4.3(tc)-4.3( )10.1(i)-4.3(alex-4.3(silf-aatterni-4.3(icng-4.3(

9. I. Jánossy, K. Fodor-Csorba, A. Vajda, and L. O. Palomares, “Light-induced spontaneous pattern formation in nematic liquid crystal cells,” Appl. Phys. Lett. (11), 111103 (2011).
10. C. Zheng and R. B. Meyer, “Thickness effects on pattern formation in liquid crystals in a rotating magnetic field,” Phys. Rev. E Stat. Phys. Plasmas Fluids Relat. Interdiscip. Topics (3), 2882–2887 (1997).
11. K. B. Migler and R. B. Meyer, “Solitons and pattern formation in liquid crystals in a rotating magnetic field,” Phys. Rev. Lett. (11), 1485–1488 (1991).
12. S. Nasuno, N. Yoshimo, and S. Kai, “Structural transition and motion of domain walls in liquid crystals under a rotating magnetic field,” Phys. Rev. E Stat. Phys. Plasmas Fluids Relat. Interdiscip. Topics (2), 1598–1601 (1995).
13. T. Frisch, S. Rica, P. Coullet, and J. M. Gilli, “Spiral waves in liquid crystal,” Phys. Rev. Lett. (10), 1471–1474 (1994).
14. J. Palacci, S. Sacanna, A. P. Steinberg, D. J. Pine, and P. M. Chaikin, “Living crystals of light-activated colloidal surfers,” Science (6122), 936–940 (2013).
15. L. Giomi, M. J. Bowick, X. Ma, and M. C. Marchetti, “Defect annihilation and proliferation in active nematics,” Phys. Rev. Lett. (22), 228101 (2013).
16. T. Sanchez, D. T. N. Chen, S. J. DeCamp, M. Heymann, and Z. Dogic, “Spontaneous motion in hierarchically assembled active matter,” Nature (7424), 431–434 (2012).
17. Y. Zhang, N. Zhou, N. Li, M. Sun, D. Kim, S. Fraden, I. R. Epstein, and B. Xu, “Giant volume change of active gels under continuous flow,” J. Am. Chem. Soc. (20), 7341–7347 (2014).
18. P. G. de Gennes and J. Prost, *The Physics of Liquid Crystals*, 2nd Ed. (Clarendon, 1993).
19. P. M. Chaikin and T. C. Lubensky, *Principles of Condensed Matter Physics* (Cambridge University, 2000).
20. A. Martinez, H. C. Mireles, and I. I. Smalyukh, “Large-area optoelastic manipulation of colloidal particles in liquid crystals using photoresponsive molecular surface monolayers,” Proc. Natl. Acad. Sci. U.S.A. (52), 20891–20896 (2011).
21. I. I. Smalyukh and O. D. Lavrentovich, “Anchoring-mediated interaction of edge dislocations with bounding surfaces in confined cholesteric liquid crystals,” Phys. Rev. Lett. (8), 085503 (2003).
22. N. Petit-Garrido, R. P. Trivedi, J. Ignés-Mullol, J. Claret, C. Lapointe, F. Sagués, and I. I. Smalyukh, “Healing of defects at the interface of nematic liquid crystals and structured Langmuir-Blodgett monolayers,” Phys. Rev. Lett. (17), 8163–8170 (2011).
23. N. Petit-Garrido, R. Trivedi, F. Sagués, J. Ignés-Mullol, and I. I. Smalyukh, “Topological defects in cholesteric liquid crystals induced by chiral molecular monolayer domains,” Soft Matter , 8163–8170 (2014).
24. P. J. Ackerman, Z. Qi, and I. I. Smalyukh, “Optical generation of crystalline, quasicrystalline, and arbitrary arrays of torons in confined cholesteric liquid crystals for patterning of optical vortices in laser beams,” Phys. Rev. E Stat. Nonlin. Soft Matter Phys. (2), 021703 (2012).
25. A. Martinez, M. Ravnik, B. Lucero, R. Visvanathan, S. Žumer, and I. I. Smalyukh, “Mutually tangled colloidal knots and induced defect loops in nematic fields,” Nat. Mater. (3), 258–263 (2014).
26. C. P. Lapointe, S. Hopkins, T. G. Mason, and I. I. Smalyukh, “Electrically driven multiaxis rotational dynamics of colloidal platelets in nematic liquid crystals,” Phys. Rev. Lett. (17), 178301 (2010).
27. Q. Liu, Y. Yuan, and I. I. Smalyukh, “Electrically and optically tunable plasmonic guest-host liquid crystals with long-range ordered nanoparticles,” Nano Lett. (7), 4071–4077 (2014).
28. P. Yeh and C. Gu, *Optics of Liquid Crystal Displays* (Willey, New York, 1999).
29. P.-Y. Wang, W. Lu, D. Yu, and R. G. Harrison, “Excitability and pattern formation in a liquid crystal Fabry-Perot interferometer,” Opt. Commun. (1-3), 127–134 (2001).
30. M. Büttiker and R. Landauer, “Nucleation theory of overdamped soliton motion,” Phys. Rev. A (3), 1397–1410 (1981).
31. F. Lonberg, S. Fraden, A. J. Hurd, and R. B. Meyer, “Field-induced transient periodic structures in nema14g]TJ0.0033 TlLy8(Fabry-)]T(a)(.5(defect

thermotropic LCs similar to the ones used in displays [18,19], a large variety of dynamic patterns, including spiral waves, have been generated by rotating magnetic fields [8–13]. Interestingly, these patterns arise in the molecular alignment field, also called director field $\mathbf{n}(\mathbf{r},t)$ [18], which is tangent to the average direction of nanometer-sized elongated LC molecules that can exhibit patterns varying as a function of spatial coordinates and time. The characteristic length scales associated with the patterns can range from tens of micrometers to millimeters while characteristic timescales are larger than the typical millisecond LC realignment times [8, 19]. In this work, we demonstrate that a rich variety of dynamic LC alignment patterns can also emerge when driven by low-intensity microscope illumination or ambient light and when the thin quasi-two-dimensional LC film is in contact with a light-responsive azobenzene monolayer [20]. The physical underpinnings behind the appearance of

r e s

action with the thermotropic nematic 4-cyano-4'-pentylbiphenyl (5CB). To mitigate the aligning effects of flow, we heat the cell to the isotropic phase and then quench back to the nematic phase. The two remaining cell edges are then sealed as well. To characterize the cell thickness locally in LC cells with in-plane director alignment, we used a Berek compensator to first precisely determine the phase retardation of initially linearly polarized light after passing the LC layer and then calculate the cell thickness using this measured retardation and the known optical refractive index anisotropy of the LC, $\Delta n = n_e - n_o \approx 0.2$, at the wavelength of the used blue illumination light [20]. Here n_e and n_o are the extraordinary and ordinary refractive indices, respectively.

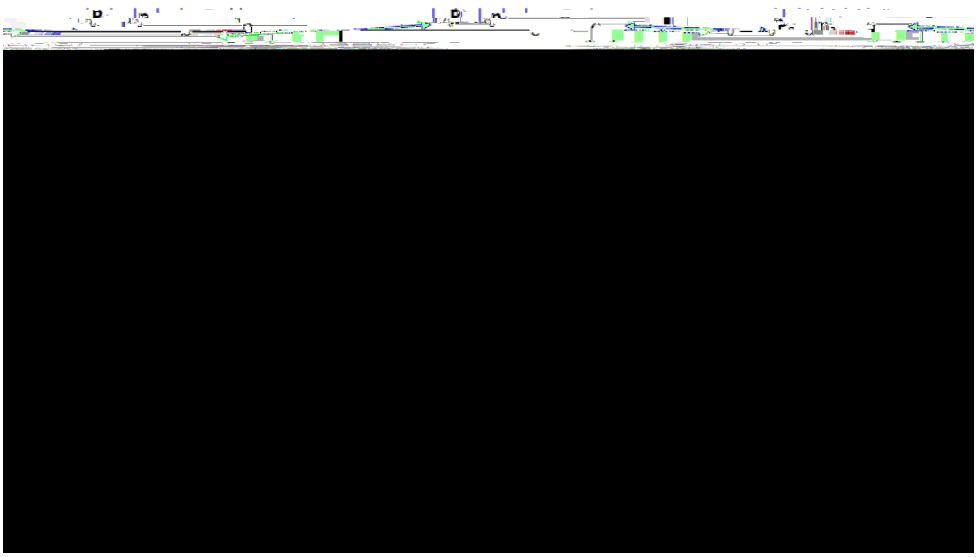

(a-f) Three types of LC cells constructed with (a, d) one substrate coated with a film of rubbed polyimide (with easy axis along the yellow arrow) and another4.1(x)-7.8(tr)-58Tc 0.1467 Tw -19.4130 Td[(ecdwith a f-1.5m)12.2(tonoaye6.2(e)rof)-7.65(he y

used to generate most of the dynamic and static patterns presented in this study. Alternatively, we also used an illumination system consisting of a LC microdisplay with 1024x768 pixels (EMP-730, Epson) that controls transmitted light intensity on a pixel-by-pixel basis, as described in details elsewhere [20]. The used illumination patterns were generated using Microsoft PowerPoint. We used objective lenses of numerical aperture within 0.1-0.9 and with magnifications ranging from 2X to 50X. To avoid modification of the controlled (,*t*) patterns while imaging them by means of transmission-mode polarizing microscopy, we minimized exposure of samples by reducing exposure time and intensity while using maximum sensitivity of the Spot 14.2 Color Mosaic Camera and an optical filter that blocks the illumination light in the blue and violet ranges of the optical spectrum, to which the DMR is most sensitive. Cells with two DMR-coated substrates can be placed on the microscope's rotation stage with either substrate facing the light source (Fig. 1). The substrate through which the normally incident light passes first will be realigned to define an easy axis perpendicular to the linear polarization orientation (or, in general, to the major axis of the elliptical polarization state), while the far substrate interacts with the complex polarization field emerging after light is transmitted through the LC film containing nonuniform (,*t*). LC cells comprising one substrate coated with rubbed polyimide or DMOAP (Fig. 1), however, are oriented so that the illumination light panh-5.8(e l1.1(0.-p defin)riza6(yi)]TJ-mid)-1.1(an)-4.8M0.-DMOAP0.0005 T

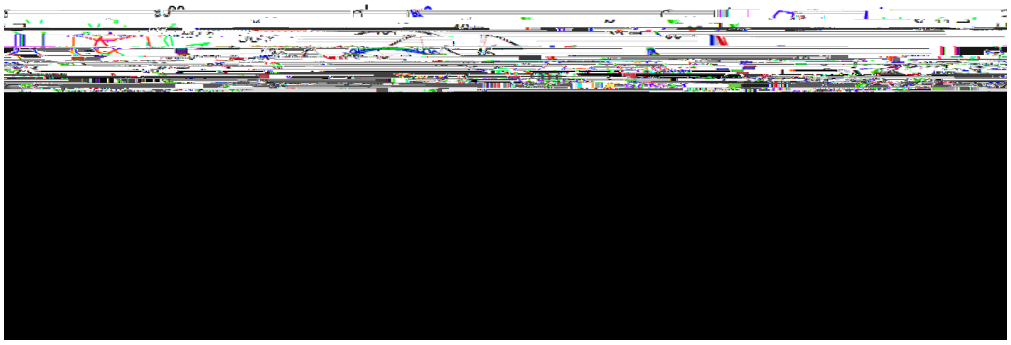

(a) A polar plot of the spiraling Néel wall coordinates in the r-θ cylindrical coordinate system at a constant time, as measured experimentally for the two spiral arms (red and blue filled circles). (b) Linear plots of r versus θ for each arm. The linear red and blue lines in (a,b) are fits of experimental data to an expression $r = r_0 + \Lambda\theta/(2\pi)$ defining the Archimedes spiral geometric configuration. The distance between consecutive solitons (wavelength) for a given

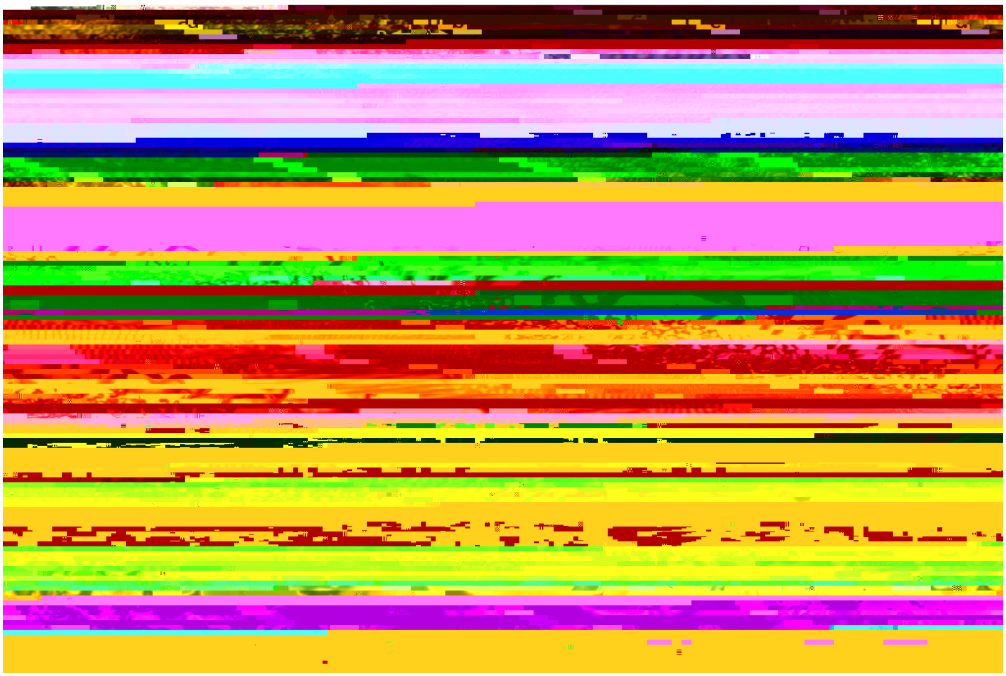

(a-l) Twelve examples of different species of observed dynamic patterns, all driven with linearly polarized white light and viewed between crossed polarizers oriented along the image edges (Media 4, Media 5, Media 6, Media 7, Media 8, Media 9, Media 10, Media 11, Media 12, Media 13, Media 14, and Media 15). The patterns (a-g) arise in thinner cells of thickness d = 1-2 μm while the patterns (h-l) are observed in thicker cells of d = 2-4 μm.

3.2. Modeling of feedback mechanisms

To obtain insights into the underlying physics responsible for the observed dynamic patterns, as an example, we consider an initially planar LC cell with the DMR-

is elliptically polarized (Fig. 1), with the azimuthal orientation, ψ, of the major axis of the polarization ellipse measured relative to the orientation of the director at the second LC-DMR interface, $_{d}(x,y,t) = (x,y,z = d,t)$; both ψ and elipticity ε are dependent on the LC film

v ——,

in the studies of field-driven dynamic patterns. In analogy with Ref [8], we can therefore write a simplified torque balance equation in the following form:

$$\xi^2 \nabla \alpha - \tau \frac{\partial \alpha}{\partial t} + \omega\tau - \sin(2\alpha) = 0. \qquad (7)$$

3.4. Effects of surface boundary conditions and lateral confinement

To uncover the elements of geometry of our photo-responsive system that are essential to observe dynamic patterns, in addition to the DMR-DMR photoalignment geometry discussed above [Figs. 1(b) and 1(e)], we have also studied cells with hybrid (homeotropic-planar) DMOAP-DMR [Figs. 1(a) and 1(d)] and planar rubbed polyimide–DMR confining surfaces [Figs. 1(c) and 1(f)]. We find that the dynamic patterns are still observed for the majority of incident linear polarization states, as long as the incident light is passed through the photoresponsive substrate after first traversing through the homeotropic or polyimide-coated confining surface and the LC film. The dynamic patterns are also robust with respect to various types of lateral confinement of the illuminated region within the plane of the LC cell (Fig. 7), although this lateral confinement is influencing selection of different dynamic pattern modes in the LC cells. To test the possible role of lateral confinement, we were driving

Although pattern formation, including Archimedes-spiral-like patterns, due to laser beams in the experimental setting of LC Fabry-Perot interferometers is known [29], it commonly requires a special setup design and laser powers of the order of tens of milliwatts. A

ordered structures in DMR monolayers but also by several types of optical dynamic patterns in terms of light's intensity, polarization state, and interference colors, all emerging from light's interaction with the dynamic structures of the director field in the LC film and polarizing optical elements (polarizer and wave plate) used in conjunction with it. It is fundamentally interesting that Archimedes spirals and other complex dynamic patterns in organization of matter and light can emerge from a spatially uniform and constant in time linear polarization of illumination light upon its interaction with the photoresponsive soft-matter system comprising a thin LC film and azobenzene self-assembled monolayer.

To conclude, we have developed a light-driven dynamic pattern-forming soft matter system that gives rise to non-equilibrium configurations and patterns in both matter and light. This self-patterning is enabled by a strongly polarization-sensitive nonlinear optical response due to an azobenzene-based alignment layer and a feedback mechanism through which the polarization state is controlled by twisted birefringent LC structures, and vice versa. A large diversity of dynamitrn i36.7(n)-1.5ncl rg
on-eunilini
e43.8(n)43.9(e)-1.2((is[1h)-49(,2h)-49(].
n etai(led)-445
(o ze(
mi40.1ingc
wlm4n g,cti4021hr5(-(dn.5e an79scrim)1025bedn.5( )5.9obn59(ervati4021ii4021
hw-ianttinsn(evn
i40.1v(e)86(rs(i40.1ti40.1yn)4.9(
(